Available online at www.sciencedirect.com
ScienceDirect
Proceedings of the Combustion Institute 000 (2022) 1–11
Proceedings of the Combustion Institute
www.elsevier.com/locate/proci

Flame evolution and radiation hazards of rectangular fires between two parallel walls

Fei Tang [a], Peng Hu [b], Jennifer X. Wen [c,*]

[a] State Key Laboratory of Fire Science, University of Science and Technology of China, Hefei, Anhui, 230026, China
[b] School of Resources and Civil Engineering, Northeastern University, Shenyang, Liaoning, 110819, China
[c] Warwick fire, School of Engineering, University of Warwick, Coventry, CV4 7AL, United Kingdom

Received 27 December 2021; accepted 5 September 2022
Available online xxx

Abstract

The manuscript investigated experimentally the influence of two parallel walls on the flame geometric parameters and radiative heat flux distributions along the wall from fires on rectangular burners. Four sets of burners with equal area and different aspect ratios were used. The burner aspect ratios, separation distance between two parallel walls and the fire heat release rates were systematically varied in the tests. Measurements were conducted for the flame height evolution and radiation hazards. The results were analysed to build the change trends of the vertical flame height and radiant heat flux with the change of the separation distance between two parallel walls. A normalized flame height equation incorporating the separation distance was proposed. The results also revealed that the radiant heat fluxes along a vertical target do not change monotonously. Comparison between the measurements and the radiant heat fluxes calculated by some published empirical models revealed relatively large discrepancies. A view factor based formula was hence proposed by assuming the flame shape as a triangular prism based on the probability flame contours for relatively larger burner aspect ratios ($n \geq 3$) and found to correlate well with the measurements.

Keywords: Rectangular fires; Aspect ratio; Flame height; Radiant heat flux; Two parallel walls

1. Introduction

Most efforts related to fire plumes have been devoted to study the flame shapes [1–3], which are determined by the geometric size of the fire source and fire heat release rate [2]. For the vertical flame extent, previous researchers focused on studying the effect of fire source shape. Yuan and Cox [4] experimentally investigated the flame length for some line fires. Hu et al. [5] proposed a global flame height model of rectangular jet fires in reduced pressure environments. Gao et al. [6] studied the flame length of slot burner fire and proposed a correlation for the flame length.

* Corresponding author at: Warwick fire, School of Engineering, University of Warwick, Gibbet Hill Rd, Coventry, CV4 7AL, United Kingdom.
E-mail address: jennifer.wen@warwick.ac.uk (J.X. Wen).

https://doi.org/10.1016/j.proci.2022.09.035

Flame radiation is also an important parameter to characterize the combustion resulted thermal hazards. There are currently three basic types of flame radiation models, namely, single point source (SPS) model, weighted-multi-point-source (WMP) model and solid flame model (SFM) [7,8]. The SPS model simply assumed the flame radiation is emitted from a point in the center of the flame volume and independent of the flame shape. As an improvement over the SPS model, the WMP model considers radiation being emitted from multiple point sources distributed along the flame axis [7]. The SFM went further to assume that the flame is a prism with the bottom of the fire source as the base, emitting uniform radiation from the entire flame surface [8]. To use the SFM, the flame surface area, and the view factor between the flame and the target need to be quantified. This is a complex function of the three-dimensional (3-D) flame shape.

However, the development of a fire plume is often restricted by external boundaries, which affect air entrainment, flame shape characteristics. Some previous show the case the wall fires have an important impact on flame geometry [9–12]. Hasemi and Tokunaga [9] conducted experiments of wall fires and studied the changes in flame shapes. Tang et al. [12] studied the ceiling jet induced by wall-attached fires in a channel and proposed a correlation for heat flux under the ceiling. Therefore, the aim of this work is to reveal and clarify the influence of the separation distance between two parallel walls and shape of the fire source itself on the flame evolution and radiation hazards. The following experimental and theoretical study aims to fill this knowledge gap.

2. The experimental setup and measurement

Fig. 1 illustrates the experimental setup. One wall was made of fireproof board of 2.4 m (height) × 2 m (width), the other was constructed with transparent glass. The fireproof board used is calcium silicate ceramic fiber board with a with a thickness of 3 cm. Its thermal conductivity is 0.18×10^{-3} kW/(m·K), density is 285 kg/m^3 and specific heat capacity is 1.39 kJ/(kg·K). Four rectangular burners with the same surface area but different aspect ratios were used to simulate from axisymmetric ($n = 1$) to line ($n = 10$) fire source. The considered aspect ratios are $n = 1$, 3, 6 and 10, respectively.

The geometric details and the experimental set up are listed in Table 1 and Table 2. The tests were carried out in ambient temperature of 15 ± 5 °C. The fire heat release rate (HRR), separation distance (D) between the two parallel walls and the burner aspect ratio (n) were systematically varied. Each test condition was repeated three times with the average measurements used for the analysis.

The burner height was 30 cm with its long side being parallel to the wall. The fuel was propane. Its supply rate, and hence the heat release rate, was controlled by a mass flow meter. Eight 150° wide-view-angle Schmidt Boelter radiometers with a range of 0–100 kW/m^2 were used to measure the flame radiation. A string of thermocouples was placed in the center above the burner to measure the centerline temperature. The lower thermocouples were spaced 3 cm apart vertically and the upper ones 15 cm apart.

Two CCD cameras were used to capture the flame evolution in the experiment. The geometric features of the fire plume were captured by the CCD camera with 1920 × 1080 pixels and 25 frames per second. For each test, 30 s of steady state original video with a constant heat release rate was decompressed into 750 consecutive frames. The captured images were processed with the image processing program to obtain the flame appearance probability. The OTSU method [13] was used to transfer the original frames into gray scale images by MATLAB. The threshold obtained was then used to identify the flame area in each image. Finally, by averaging all the captured frames, the mean visible flame appearance probability can be obtained and converted back into color contours.

3. Results and discussion

3.1. Flame height of rectangular fires between two parallel walls

Fig. 2 shows flame images at different instantaneous times for the different burners. The flame height was found to gradually decrease with the increase of the burner aspect ratio.

Some dark regions can be seen in Fig. 2 near the burner surface and more clearly in Fig. 3(a) and (b) which zoomed in on two of the frames. This was found to be the case for all the videos captured under different shooting angles and geometric arrangements (Fig. 3(c), (d) and (e)).

Dark regions are also seen in Fig. 4 probability contours. The measured centerline temperature rise is plotted in Fig. 5(a) for the burner with aspect ratio $n = 1$ and $D = 0.3$ m, where the abscissa is $(\frac{Z}{\dot{Q}^{2/5}})^{\eta}$, ΔT is the temperature rise, Z is the distance above the burner surface, $\dot{Q}$ is the fire heat release rate, η is the exponential constant corresponding to different flame zones proposed by McCaffrey [14]. The distribution of the temperature rise was divided into three regions, i.e. the continuous flame, intermittent flame and the plume regions. The present measurements for the later part of the continuous flamen region, the intermittent flame and plume regions agree well with the measurements of McCaffrey [14]. For the lower regions of the continuous flame region, the present

Please cite this article as: F. Tang, P. Hu and J.X. Wen, Flame evolution and radiation hazards of rectangular fires between two parallel walls, Proceedings of the Combustion Institute, https://doi.org/10.1016/j.proci.2022.09.035

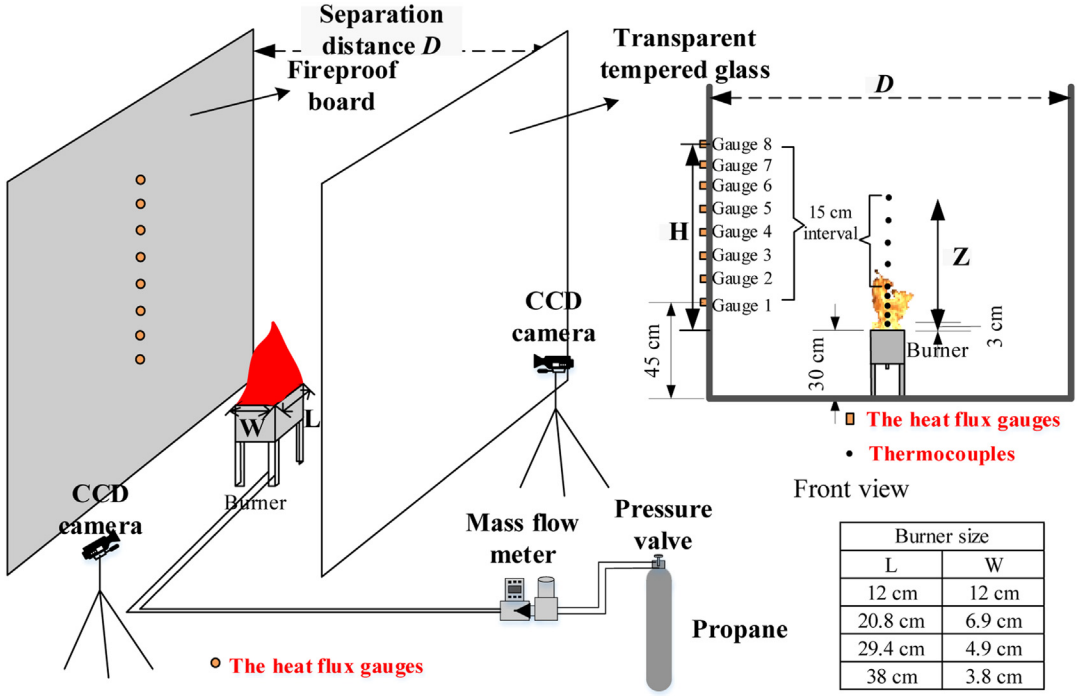

Fig. 1. The experimental setup.

Table 1
Experimental conditions with parallel walls.

Test no.	Burner size $L \times W$ (cm × cm)	Aspect ratio n ($n = L/W$)	Separation distance between two parallel walls D (m)	Mass flow rate (kg/s)	HRRs (kW)	*Re* number
1–16	12 × 12	1	0.3, 0.6, 0.9, 1.2	0.142×10^{-3} ~0.563×10^{-3}	7.2; 14.1; 21.3; 28.1	3.76×10^4 ~4.93×10^4
17–32	20.8 × 6.9	3	0.3, 0.6, 0.9, 1.2	0.142×10^{-3} ~0.563×10^{-3}	7.2; 14.1; 21.3; 28.1	3.24×10^4 ~4.26×10^4
33–48	29.4 × 4.9	6	0.3, 0.6, 0.9, 1.2	0.142×10^{-3} ~0.563×10^{-3}	7.2; 14.1; 21.3; 28.1	2.63×10^4 ~3.45×10^4
49–64	38 × 3.8	10	0.3, 0.6, 0.9, 1.2	0.142×10^{-3} ~0.563×10^{-3}	7.2; 14.1; 21.3; 28.1	2.16×10^4 ~2.84×10^4

Table 2
Experimental conditions without parallel walls.

Test no.	Burner size $L \times W$ (cm × cm)	Aspect ratio n ($n = L/W$)	Distance between burner center and measuring point (m)	Mass flow rate (kg/s)	HRRs (kW)	*Re* number
65–80	12 × 12	1	0.15, 0.3, 0.45, 0.6	0.142×10^{-3} ~0.563×10^{-3}	7.2; 14.1; 21.3; 28.1	3.76×10^4 ~4.93×10^4
81–96	20.8 × 6.9	3	0.15, 0.3, 0.45, 0.6	0.142×10^{-3} ~0.563×10^{-3}	7.2; 14.1; 21.3; 28.1	3.24×10^4 ~4.26×10^4
97–112	29.4 × 4.9	6	0.15, 0.3, 0.45, 0.6	0.142×10^{-3} ~0.563×10^{-3}	7.2; 14.1; 21.3; 28.1	2.63×10^4 ~3.45×10^4
113–128	38 × 3.8	10	0.15, 0.3, 0.45, 0.6	0.142×10^{-3} ~0.563×10^{-3}	7.2; 14.1; 21.3; 28.1	2.16×10^4 ~2.84×10^4

Please cite this article as: F. Tang, P. Hu and J.X. Wen, Flame evolution and radiation hazards of rectangular fires between two parallel walls, Proceedings of the Combustion Institute, https://doi.org/10.1016/j.proci.2022.09.035

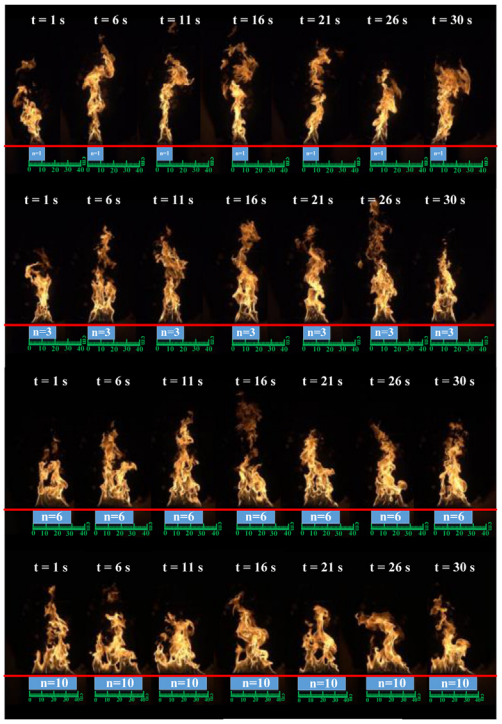

Fig. 2. The captured flames images at different instantaneous times for the different burners. (HRR = 28.1 kW, $D = 0.3$ m).

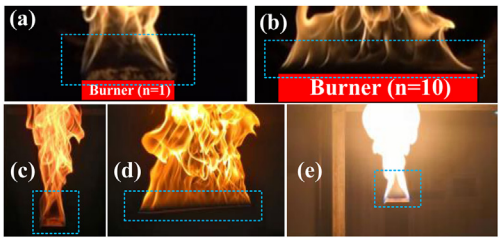

Fig. 3. Partial enlarged view near the flame bases for the different burners (HRR = 28.1 kW, $D = 0.3$ m).

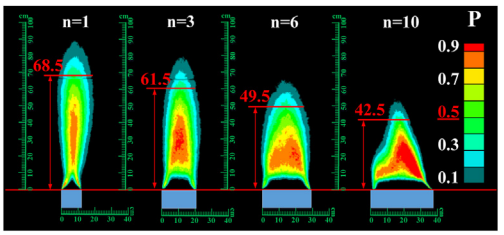

Fig. 4. Flame appearance probability contour for the different burners (HRR = 28.1 kW, $D = 0.3$ m).

measurements shown different trends than that of McCaffrey [14], i.e. the temperatures continued to drop towards the burner surface quite rapidly. This indicates that there is little or no flame burning in the central area near the burner surface due to lack of sufficient mixing of the fuel with fresh air.

In addition to the constraints of the two parallel walls, which restrict air entrainment into the combustion region, the present experiments used propane, which has higher carbon content than natural gas used in McCaffrey's experiments [14]. Although the stoichiometric air to fuel ratios by mass for propane and natural gas are similar, the stoichiometric air to fuel ratio by volume for propane at 26.11 is more than twice the value for methane (~10.42). Even though the actual air fuel ratio by volume may be slightly higher for natural gas which contains small amounts of higher hydrocarbons, this significant difference still means that higher volume of air needs to be entrained to mix with the fuel and sustain combustion. This is challenging near the base of the flame as the flame velocity is very low and going through the transition from laminar to turbulent flow. The constraint of the two parallel walls restricts air entrainment even further. As fresh air cannot diffuse to the center near the flame base [15], the region is extremely fuel rich with incomplete combustion. It causes the centerline temperature near the burner base to be lower than the measurements of McCaffrey [14] as shown in Fig. 5(b).

Based on the above findings, it is necessary to carry out a physical modeling analysis of the air entrainment mode of flame combustion under the restriction of parallel walls. Fig. 6 illustrates the physical mechanism of the restricted air entrainment. In open flame, the entrainment condition is the same on all sides, the fire plume entrainment is not limited. Between two parallel walls, more air is entrained from the unrestricted ends and is restricted by the two parallel walls to move upwards (Fig. 6(b)). The flame velocity is always vertically upward, while the entrainment velocity is proportional to the flame velocity, and the entrainment velocity is equal to the flame velocity multiplied by the entrainment coefficient.

$$V_e = \alpha V_f \tag{1}$$

where V_e is air entrainment velocity, α is the air entrainment coefficient, V_f is flame velocity.

For the air mass flow required for fuel combustion, each position of the flame should be different, which can be calculated by the following integral equation.

$$d\dot{m} = \rho_a V_e dA \tag{2}$$

where ρ_a is the environmental air density, dA is the area through which entrainment takes place.

Due to the use of a rectangular burner, the flame shape is rectangular, which can further simplify the

Please cite this article as: F. Tang, P. Hu and J.X. Wen, Flame evolution and radiation hazards of rectangular fires between two parallel walls, Proceedings of the Combustion Institute, https://doi.org/10.1016/j.proci.2022.09.035

integral by combining Eq. (1) and Eq. (2). For a flame flow produced by a rectangular burner, the entrained air at height x is,

$$\dot{m}_x = \int_0^x \rho_a \alpha V_f (2L + 2W) dx \tag{3}$$

Since the main consideration is the flame shape that affects air entrainment to flame, the detailed entrainment calculations can be approximated and simplified. Therefore, it is necessary to summarize the factors that affect the air entrainment to the fire plume. When the flame is not restricted, the air entrainment is related to the side length of the burner in different directions, which can be expressed as:

$$\dot{m}_L \sim \alpha L \tag{4a}$$

$$\dot{m}_W \sim \alpha W \tag{4b}$$

where α is the air entrainment coefficient, $\dot{m}_L$ and $\dot{m}_W$ are the air entrainment rate of burner's length and width, thus, the total air entrainment rate of the flame under unlimited conditions can be obtained:

$$\dot{m}_{total} \sim 2\alpha(L + W) \tag{5}$$

When the two sides of the flame are restricted by the walls, air entrainment is affected by the distance between the parallel walls. The non-dimensional distance influence factor $1 - W/D$ is used to characterize the effect of the parallel walls, and the air entrainment rate on the restricted side is:

$$\dot{m}'_L \sim \alpha L(1 - W/D) \tag{6}$$

The total air entrainment rate under wall restriction is:

$$\dot{m}'_{\text{total}} \sim 2\alpha(\text{L}(1 - W/\text{D}) + W)$$

$$\dot{m}'_{\text{total}} \sim 2\alpha(L(1 - W/D) + W) \tag{7}$$

As the flame height is inversely proportional to the air entrainment rate, the flame height influence

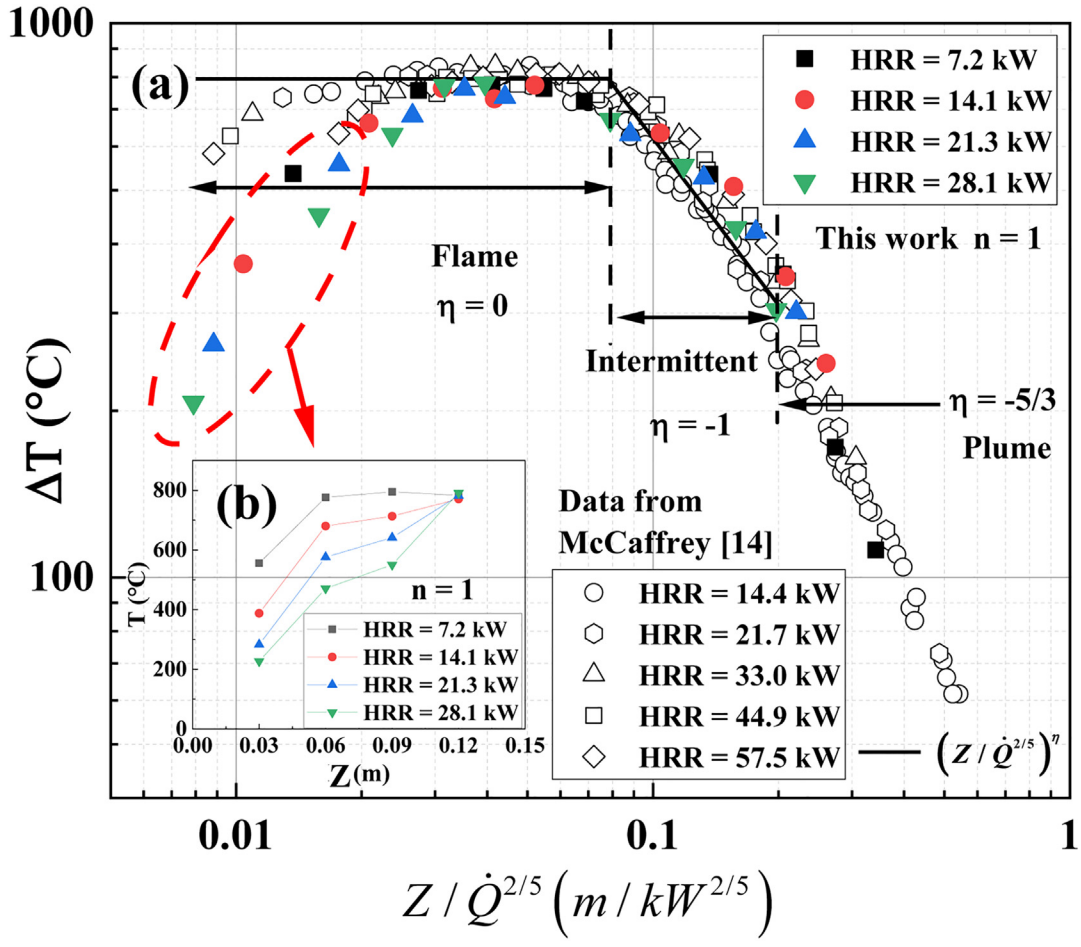

Fig. 5. Centerline temperature distribution ($n = 1$, $D = 0.3$ m).

Please cite this article as: F. Tang, P. Hu and J.X. Wen, Flame evolution and radiation hazards of rectangular fires between two parallel walls, Proceedings of the Combustion Institute, https://doi.org/10.1016/j.proci.2022.09.035

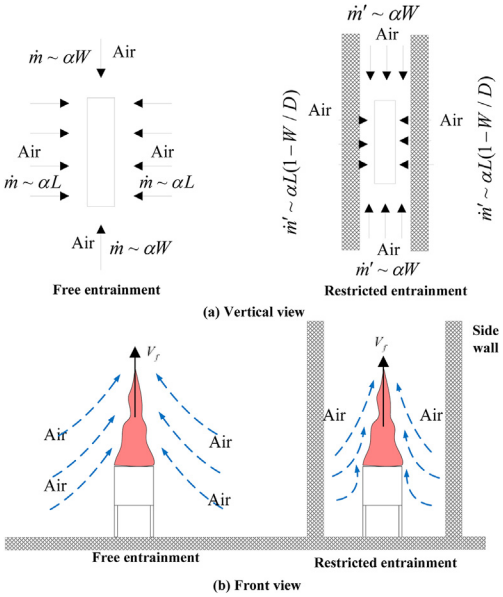

Fig. 6. Physical mechanism of restricted air entrainment.

factor K can be calculated as:

$$K = \frac{\dot{m}_{total}}{\dot{m}'_{total}} = \frac{2\alpha(L+W)}{2\alpha(L(1-W/D)+W)} \tag{8}$$

In previous work, it has been shown that the presence of parallel walls and their separation distance will strongly block the entrainment of fresh air from side direction into the flame and thus influence the flame height [16]. Fig. 7 show the flame height evolution with HRR under different separation distance between two parallel walls. The flame height increases with the decrease of the distance between the walls. It decreases with the increases of the burner aspect ratio. The results evidence the strong restrictive effect of the walls on air entrainment and thus the flame height. To capture this effect with a simple correlation, it is proposed to normalize the flame height under different distance beside two parallel walls.

For free flame height, extensive studies have confirmed that H_f/D^* is a function of $\dot{Q}^*_{D^*} = \dot{Q}/(\rho_\infty T_\infty c_p g^{1/2} D^{*5/2})$ for axisymmetric burners, the function of flame height is:

$$H_f/D^* \sim f\left(\dot{Q}^*_{D^*}\right) \tag{9}$$

Where $\dot{Q}$ is heat release rate, ρ_∞ is air density, c_p is specific heat capacity, T_∞ is ambient temperature, g is gravitational acceleration, D^* is the hydraulic diameter of the burner.

According to previous studies [17], flame height is affected by air entrainment around the ignition source. For an unrestricted free fire, the flame height is related to the circumference of the fire source. When the flame shape changes, such as an increase in the burner aspect ratio, the flame height decreases as large aspect ratio burner has a larger perimeter to entrain more air, which decreases the flame height. Therefore, the flame height was analyzed using the perimeter $C^* = 2(L+W)$ as the characteristic diameter. The form of non-dimensional fire heat release rate can be expressed as $\dot{Q}^*_{C^*} = \dot{Q}/(\rho_\infty T_\infty c_p g^{1/2} C^{*5/2})$. Eq. (9) can be modified as:

$$H_f/C^* \sim f\left(\dot{Q}^*_{c^*}, K\right) \tag{10}$$

Based on the analysis, it is assumed that the non-dimensional heat release rate has a 2/3-order function relationship with the non-dimensional flame height, which is consistent with previous studies. As shown in Fig. 8, the final relationship can be obtained by normalizing and analyzing all the experimental data:

$$\frac{H_f}{C^* \cdot K} = 3.95\left(\frac{\dot{Q}}{\rho_\infty T_\infty c_p \sqrt{g} C^{*5/2}}\right)^{2/3} \tag{11}$$

There are two different functional relationships for flame height. In the region dominated by two-dimensional entrainment, the flame height is related to the 2/3 power of the dimensionless heat release rate; in the region dominated by three-dimensional entrainment, the flame height is related to the 2/5 power of the dimensionless heat release rate. The previous experimental data of Hasemi and Nishihata [18], Hu et al. [19] were added for comparison, and it is found that the correlation agrees well with these measurements in the corresponding two-dimensional entrainment-dominated region.

3.2. Flame radiation hazards

As discussed earlier, the change in the burner aspect ratio affects the flame shape and thus the flame radiation hazards, which are also affected by the separation distance between the two parallel walls.

As shown in Fig. 9, the vertical radiant heat flux profile along the wall with vertical position don't change monotonously. It increases slightly with the increase of the vertical position and then decreases rapidly with further increase of the vertical position. Secondly, when the fire source is confined within two parallel walls, the vertical radiant heat flux along the vertical wall is greater than that on the same location for open flame situation. Finally, as the separation distance between the parallel walls increases, the difference between the restricted and unrestricted radiant heat flux on both sides becomes smaller.

As discussed earlier, the simplification of the SPS model renders it only suitable for estimating radiation hazards further away from the fire source. The WMP model requires the location and weighting of each point source, making it cumbersome to use.

Please cite this article as: F. Tang, P. Hu and J.X. Wen, Flame evolution and radiation hazards of rectangular fires between two parallel walls, Proceedings of the Combustion Institute, https://doi.org/10.1016/j.proci.2022.09.035

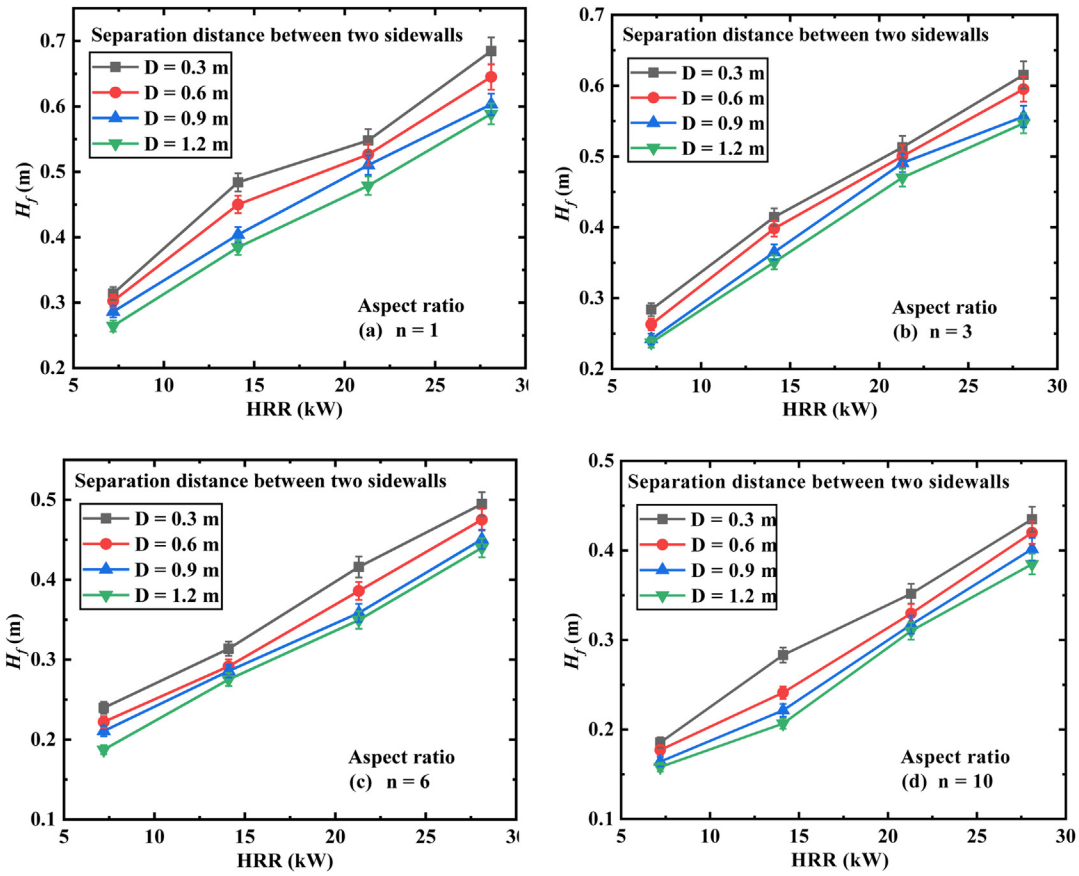

Fig. 7. Flame height evolution with HRR between two parallel walls with different separation distances.

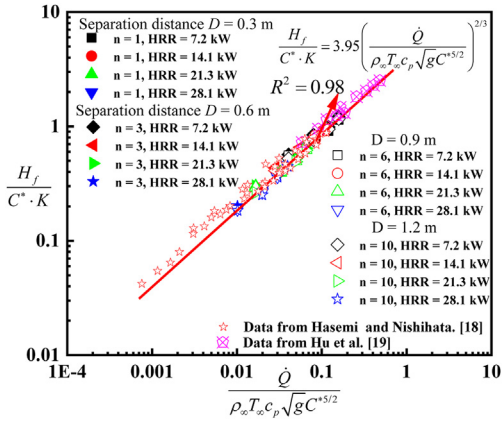

Fig. 8. The normalized flame height correlation including the effect of separation distance between two parallel walls.

For the SPS model, the radiative heat flux on a vertical target can be calculated by:

$$\dot{q}'' = \frac{\tau \dot{Q}_r cos\varphi}{4\pi R^2} \tag{12}$$

where τ is atmospheric transmissivity, $\dot{Q}_r$ is total flame radiation release rate, $\dot{Q}_r = \chi_{rad}\dot{Q}$, $cos\varphi = x_0/R$, x_0 is the horizontal distance from the target to the center of the fire source, R is the distance from the target to the center of the fire source. Also, the radiation fraction χ_{rad} can be expressed as the following [20]:

$$\chi_{rad} = \frac{\sigma T_f^4 \left(1 - e^{\kappa L}\right) A}{\dot{Q}} \tag{13}$$

where κ is the absorption coefficient, and L is the effective radiative path length, $L = 3.6V_f/A$, V_f is the flame volume, A is the flame surface area, σ is the Stefan-Boltzmann constant, T_f is the flame temperature.

For the SFM, it assumes that the flame is a cube with the same side length, and the heat radiation is evenly emitted through the flame. The thermal radiation heat flux $\dot{q}''$ to the external target is:

$$\dot{q}'' = \tau F E \tag{14}$$

where F is the view factor, E is flame surface emissive power (FSEP).

Please cite this article as: F. Tang, P. Hu and J.X. Wen, Flame evolution and radiation hazards of rectangular fires between two parallel walls, Proceedings of the Combustion Institute, https://doi.org/10.1016/j.proci.2022.09.035

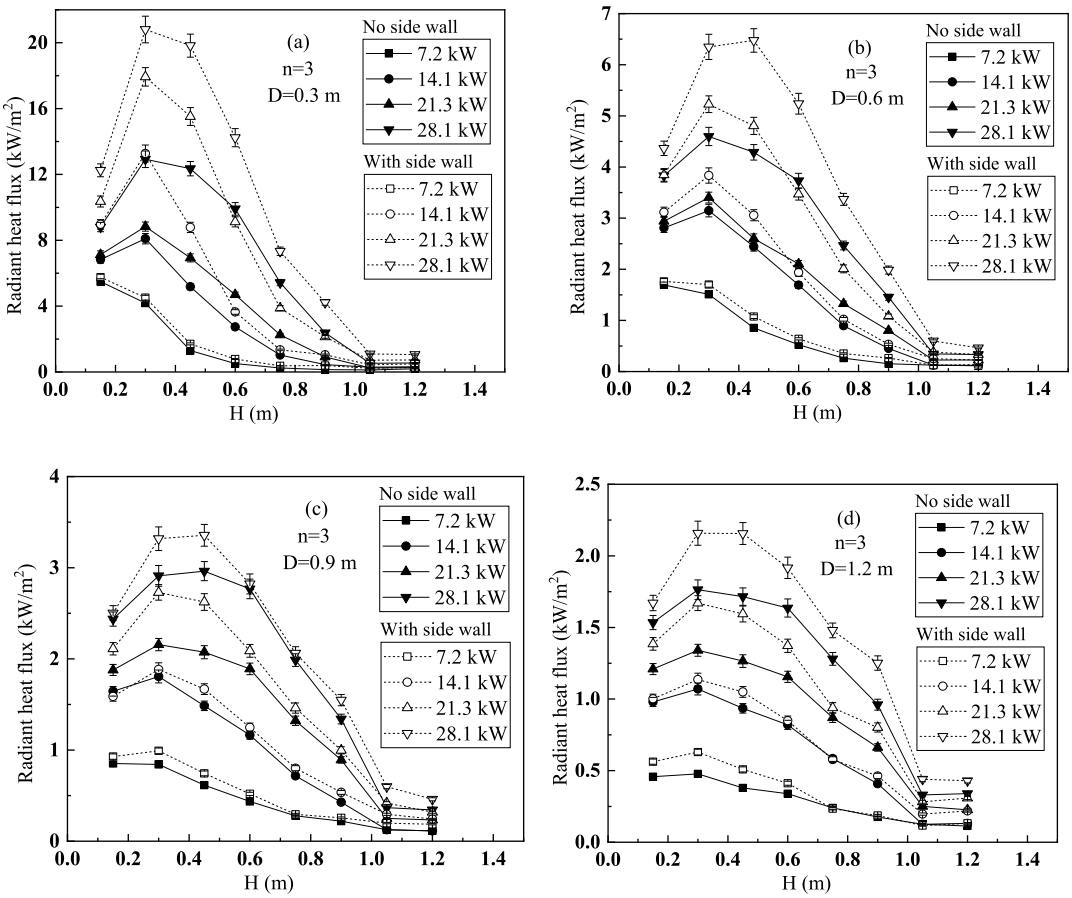

Fig. 9. The radiant heat flux distribution on the vertical wall varies with HRR with or without parallel walls ($n = 3$).

The classical SFM determines the FSEP in a simple way, which gives:

$$E = \frac{\chi_r \dot{Q}}{A} \tag{15}$$

Following Modak's work [21], the radiant fraction of buoyant flame can be regarded as a constant regardless of HRR and burner size. In this study, the flame radiant fraction χ_r is set as 0.30.

For the cuboid model, when the vertically oriented target is at one corner of the cuboid, the view factor between the cuboid and the target [22] is:

$$F_{cuboid} = \frac{1}{2\pi}\left(\frac{H_1}{\sqrt{H_1^2+x^2}}tan^{-1}\left(\frac{W_1}{\sqrt{H_1^2+x^2}}\right) + \frac{W_1}{\sqrt{W_1^2+x^2}}tan^{-1}\left(\frac{H_1}{\sqrt{W_1^2+x^2}}\right)\right) \tag{16}$$

where W_1 and H_1 are the width and height of the cuboid, and x is the horizontal distance to the target.

For the cylinder model, when the vertically oriented target is in the middle of the cylinder, the view factor of the cylinder to the target is [23]:

$$F_{cylinder} = \frac{1}{\pi Q}tan^{-1}\left(\frac{R}{\sqrt{Q^2-1}}\right) - \frac{R}{\pi Q}tan^{-1}\left(\sqrt{\frac{Q-1}{Q+1}}\right) + \frac{PR}{\pi Q\sqrt{P^2-1}}tan^{-1}\left(\sqrt{\frac{(P+1)(Q-1)}{(P-1)(Q+1)}}\right) \tag{17}$$

where these parameters are defined as $P = \frac{Q^2+R^2+1}{2Q}$, $Q = \frac{2x}{D1}$, $R = \frac{2H_1}{D1}$, $D1$ is the equivalent diameter, H_1 is the height of the cylinder, and x is the horizontal distance from the cylinder to the target. Since the radiometer has a measuring viewing angle of 150°, the upper part of the measuring point is not all in the measuring range when the fire source is

Please cite this article as: F. Tang, P. Hu and J.X. Wen, Flame evolution and radiation hazards of rectangular fires between two parallel walls, Proceedings of the Combustion Institute, https://doi.org/10.1016/j.proci.2022.09.035

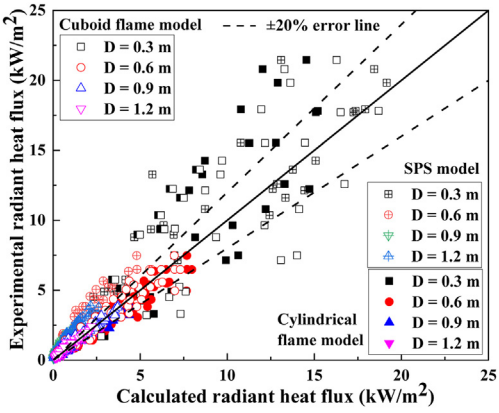

Fig. 10. Comparison between the calculated radiant heat fluxes based on some previous calculation models of flame heat radiation and the measurement.

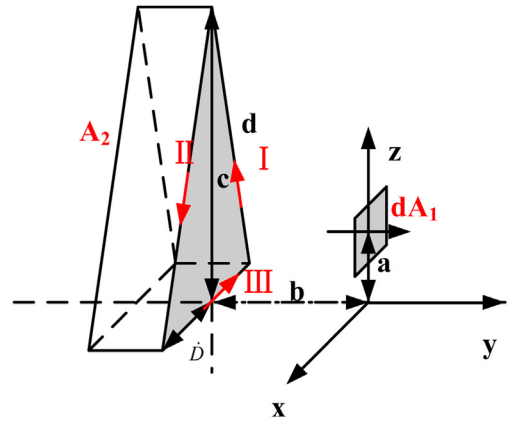

Fig. 11. The triangular prism to approximate the flame shape.

close to the wall. When the separation distance is 0.15 m, the three lower measuring points are all within the measuring range. When the distance is 0.3 m, the five lower measuring points are within the range. When the distance is 0.45 m and 0.6 m, all the measuring points are within the measuring range. The measurements within the measuring range for the burner aspect ratios of $n = 3$, 6 and 10 are thus used and substituted into the cylinder model and the cuboid flame model.

As shown in Fig. 10, the predictions are very scattered. None of the SPS model, cylindrical model and cuboid flame model can capture the vertical radiant heat flux along the wall, which was induced by rectangular fire sources with large aspect ratios. The relative error also increases with the decrease of the separation distance between the two parallel walls due to deviation of the flame shape from that of a square fire source.

For large burner aspect ratio, the flame shape can be approximated as triangular prism based on the flame probability contour in Fig. 4. The key dimensions are illustrated in Fig. 11.

Based on the contour integral method of estimating the view factor to apply Stokes' theorem to transform many integrations over a surface area into a tractable two-dimension contour integration around the boundary of the flame surface area [24], the view factor between the triangular prism and the target is illustrated in Fig. 11. Thview factor, F is given by:

$$F_{d1-2} = \frac{1}{2\pi}\oint \frac{x_2 dz_2 - z_2 dx_2}{x_2^2 + y_2^2 + z_2^2} = \frac{1}{2\pi}\int_0^d \frac{\frac{(a-c)\dot{D}}{d}d\xi}{\dot{D}^2 * \left(1-\frac{\xi}{d}\right)^2 + b^2 + \left(\frac{c\xi}{d} - a\right)^2} + \frac{1}{2\pi}\int_0^d \frac{\frac{(a-c)\dot{D}}{d}d\xi}{\frac{\dot{D}^2\xi^2}{d^2} + b^2 + \left(\left(1-\frac{\xi}{d}\right) * c - a\right)^2} + \frac{1}{2\pi}\int_{\dot{D}}^{-\dot{D}} \frac{ad\xi}{\xi^2 + b^2 + a^2} \tag{18}$$

where, b, c, d, $\dot{D}$ are used to represent some characteristic sizes/distances. a is the vertical position of the measuring point, b is the horizontal distance from the measuring point to the flame surface, c is the height of the flame, d is the length of the hypotenuse of the triangle model, $\dot{D}$ is half of the long side of the burner. Eq. (18) can thus be written as:

$$F_{1-2} = \frac{(a-c)\dot{D}}{\pi\sqrt{(a-c)^2\dot{D}^2 + b^2(c^2+\dot{D}^2)}} * \left(\tan^{-1}\left(\frac{-ac+c^2}{\sqrt{(a-c)^2\dot{D}^2 + b^2(c^2+\dot{D}^2)}}\right) + \tan^{-1}\left(\frac{ac+\dot{D}^2}{\sqrt{(a-c)^2\dot{D}^2 + b^2(c^2+\dot{D}^2)}}\right)\right) - \frac{a}{\pi\sqrt{a^2+b^2}}\tan^{-1}\left(\frac{\dot{D}}{\sqrt{a^2+b^2}}\right) \tag{19}$$

It is worth noting that the flame body may be affected by the boundary layer flow when the HRR is small, and the flame belongs to the laminar flow area. In order to ensure that the flame in the boundary layer flow is in the transitional region or the turbulent region, the local Grashof number ($Gr_h = g\beta(T_f - T_\infty)\frac{H_f}{\nu^2}$) is calculated, which refers to the ratio of the buoyant to momentum force, ν is where β is the thermal expansion coefficient, and kinematic viscosity. The critical region Gr=7.52×10^8 [25]). Through further analysis for the critical Gr. Combining Eq. (11), in order to ensure that the flame tip is in the critical region, the range of test conditions corresponding to the calculation results of this work is, $\dot{Q}^*_{C^*} \geq 0.014$.

Please cite this article as: F. Tang, P. Hu and J.X. Wen, Flame evolution and radiation hazards of rectangular fires between two parallel walls, Proceedings of the Combustion Institute, https://doi.org/10.1016/j.proci.2022.09.035

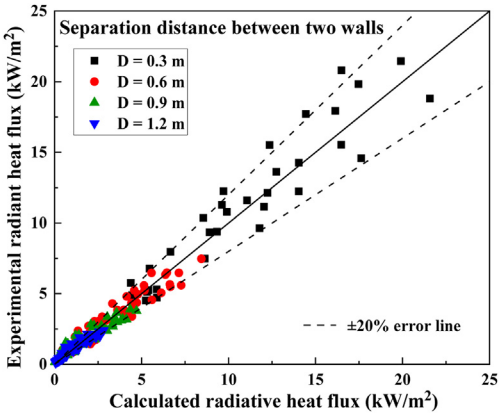

Fig. 12. Comparison between the calculated and measured radiative heat fluxes for the cases within two parallel walls.

As displayed in Fig. 12, the radiation measurements for the burners with aspect ratios of $n = 3$, 6 and 10 were subsequently analyzed by substituting the measured values into the triangular prism model. To consider the different flames shapes associated with different burner aspect ratios, the view factor was modified accordingly. The calculated radiation fluxes are thus different from the previous models. The calculated vertical radiative heat fluxes along the wall by the newly proposed model with modified view factor (Eq. (19)), as shown in Fig. 12, are within 20% of the measurements.

4. Conclusions

The flame geometric evolution and flame radiation hazards of rectangular fires with different aspect ratios between two parallel walls was studied. A series of experiments were carried out by changing the HRRs, separation distance between two walls and burner aspect ratios. The main findings include:

(1) Comparing with open diffusion flames, the lower part of the persistent flame region exhibited much lower temperatures due to the presence of the two parallel walls to restrict air entrainment into the core region. The higher stoichiometric air fuel ratio by volume of propane in comparison with natural gas further contributes to the oxygen deficiency in the core neat the base of the flame.
(2) When the fire source is between two parallel walls, the flame height increases with the decrease of the separation distance between the two parallel walls, and decreases with the increase of the burner aspect ratio due to the restricted air entrainment. A normalized flame height formula incorporating the separation distance between the two parallel walls is proposed.
(3) A view factor based formula was proposed by assuming the flame shape as a triangular prism based on the probability flame contours for relatively larger burner aspect ratios ($n \geq 3$). Its calculated radiative heat fluxes along the wall were in good agreement with the experimental results.

Declaration of Competing Interest

The authors declare that they have no known competing financial interests or personal relationships that could have appeared to influence the work reported in this paper.

Acknowledgements

This work was supported by the National Natural Science Foundation of China under Grant Nos. 52076066 and 52211530053, Anhui Provincial Natural Science Foundation (No. 2208085J34), CAS Pioneer Hundred Talents Program to Dr. Fei Tang, Program for Foreign Experts Introduction of Anhui Province and International Visiting Professor Program (No. 2021BVR04).

References

[1] F. Tang, Q. He, J. Wen, Effects of crosswind and burner aspect ratio on flame characteristics and flame base drag length of diffusion flames, Combust. Flame 200 (2019) 265–275.
[2] G. Heskestad, Luminous heights of turbulent diffusion flames, Fire Saf. J. 5 (2) (1983) 103–108.
[3] F. Tang, L. Deng, L. Chen, Q. Wang, Effects of burner aspect ratio on heat flux distributions beneath unconfined ceilings with different inclination angles, Combust. Flame 228 (2021) 99–106.
[4] L.M. Yuan, G. Cox, An experimental study of some line fires, Fire Saf. J. 27 (2) (1996) 123–139.
[5] L.H. Hu, X.C. Zhang, X.L. Zhang, K.H. Lu, Z.M. Guo, Flame heights and fraction of stoichiometric air entrained for rectangular turbulent jet fires in a sub-atmospheric pressure, Proc. Combust. Inst. 36 (2) (2017) 2995–3002.
[6] W. Gao, N.A. Liu, Y. Jiao, X.D. Xie, Y. Pan, Z.L. Li, X.S. Luo, L.H. Zhang, R. Tu, Flame length of buoyant turbulent slot flame, Proc. Combust. Inst. 37 (3) (2019) 3851–3858.
[7] R.B. Miguel, I.M. Machado, F.M. Pereira, P.R. Pagot, F.H.R. França, Application of inverse analysis to correlate the parameters of the weighted-multi-point-source model to compute radiation from flames, Int. J. Heat Mass Transf. 102 (2016) 816–825.
[8] K.S. Mudan, Geometric view factors for thermal radiation hazard assessment, Fire Saf. J. 12 (1987) 89–96.

Please cite this article as: F. Tang, P. Hu and J.X. Wen, Flame evolution and radiation hazards of rectangular fires between two parallel walls, Proceedings of the Combustion Institute, https://doi.org/10.1016/j.proci.2022.09.035

[9] Y. Hasemi, T. Tokunaga, Some experimental aspects of turbulent diffusion flames and buoyant plumes from fire sources against a wall and in a corner of walls, Combust. Sci. Technol. 40 (1984) 1–18.
[10] M. Poreh, G. Garrad, A study of wall and corner fire plumes, Fire Saf. J. 34 (2000) 81–98.
[11] X. Jiang, K.H. Luo, Dynamics and structure of transitional buoyant jet diffusion flames with side-wall effects, Combust. Flame 133 (1–2) (2003) 29–45.
[12] F. Tang, P. Hu, J. Zhang, J. Wen, Heat fluxes under the ceiling induced by wall fires with various burner aspect ratios in a channel, Proc. Combust. Inst. 38 (3) (2021) 4567–4577.
[13] N. Otsu, A threshold selection method from gray-level histograms, IEEE Trans. Syst. Man Cybern. 9 (1979) 62–66.
[14] B.J. McCaffrey, Purely Buoyant Diffusion Flames: Some Experimental Results, NBSIR 79-1910, National Bureau of Standards, October 1979.
[15] G. Cox, R. Chittya, Study of the deterministic properties of unbounded fire plumes, Combust. Flame 39 (1980) 191–209.
[16] K.H. Lu, L.H. Hu, F. Tang, L.H. He, X.C. Zhang, Z.W. Qiu, Experimental investigation on window ejected facade flame heights with different constraint side wall lengths and global correlation, Int. J. Heat Mass Transf. 78 (2014) 17–24.
[17] X.L. Zhang, X. Fang, L.H. Hu, Buoyant turbulent diffusion flame heights of free, wall and corner air entrainment conditions: experiments and global model based on mirror approach, Fuel 303 (2021) 121338.
[18] Y. Hasemi, M. Nishihata, Fuel shape effect on the deterministic properties of turbulent diffusion flames, in: Fire Safety Science-Proceedings of the Second International Symposium, 38, 1989, pp. 29–34.
[19] L.H. Hu, S.X. Liu, X.L. Zhang, Flame heights of line-source buoyant turbulent non-premixed jets with air entrainment constraint by two parallel side walls, Fuel 200 (2017) 583–589.
[20] M.J. Hurley, D.T. Gottuk, J.R. Hall Jr, K. Harada, E.D. Kuligowski, M. Puchovsky, J.M. Watts Jr, C.J. WIECZOREK, SFPE Handbook of Fire Protection Engineering, Springer, 2015.
[21] A.T. Modak, Thermal radiation from pool fires, Combust. Flame 29 (1977) 177–192.
[22] H. Ingason, Y.Z. Li, A. Lönnermark, Heat flux and thermal resistance, in: Tunnel Fire Dynamics, Springer, New York, 2015, pp. 249–290.
[23] C.L. Beyler, Fire hazard calculations for large, open hydrocarbon fires. SFPE handbook of fire protection engineering, in: National Fire Protection Association, 5th ed, Springer, Quincy, 2016, pp. 2591–2663.
[24] J.R. Howell, M.P. Menguc, R. Siegel, Configuration Factors for Diffuse Surfaces With Uniform Radiosity, Thermal radiation Heat Transfer, CRC press, 2010.
[25] K. Noto, K. Teramoto, T. Nakajima, Spectra and critical Grashof numbers for turbulent transition in a thermal plume, J. Thermophys. Heat Tr. 13 (1999) 82–90.

Please cite this article as: F. Tang, P. Hu and J.X. Wen, Flame evolution and radiation hazards of rectangular fires between two parallel walls, Proceedings of the Combustion Institute, https://doi.org/10.1016/j.proci.2022.09.035